NUMERICAL SIMULATION OF ATMOSPHERIC FLOW OVER AN IDEALIZED MOUNTAIN

by

James Keith DeBoer

United States
Naval Postgraduate School

THESIS

NUMERICAL SIMULATION OF ATMOSPHERIC FLOW
OVER AN IDEALIZED MOUNTAIN

by

James Keith DeBoer

September 1970

This document has been approved for public release and sale; its distribution is unlimited.

Numerical Simulation of Atmospheric Flow Over an Idealized Mountain

by

James Keith DeBoer
Lieutenant, United States Navy
B.S., Illinois Institute of Technology, 1963

Submitted in partial fulfillment of the
requirement for the degree of

MASTER OF SCIENCE IN METEOROLOGY

from the

NAVAL POSTGRADUATE SCHOOL
September 1970

ABSTRACT

The validity of linear smoothing of topography for numerical weather prediction and the variation of mountain drag with mountain height and static stability are examined in this study. In the model a constant geostrophic current is perpendicular to the mountain range and the height of the mountain is independent of y. The hydrostatic Boussinesq equations are used with motion bounded at the top by a rigid plane at z = D. A modified coordinate system similar to Phillips' sigma system was used. Solutions were obtained using a smoothed mountain profile. These solutions were compared with smoothed solutions obtained from the unsmoothed mountain. The comparison of these solutions shows that an error is introduced when non-linear terms become sufficiently large. Values of the mountain drag for differing values of mountain height at a given static stability and for differing values of static stability at a given mountain height were computed. Mountain drag was found to vary quadratically with mountain height and linearly with static stability.

TABLE OF CONTENTS

LIST OF FIGURES

LIST OF SYMBOLS

B	Mountain amplitude
c_p	Specific heat of air at constant pressure
D	Maximum depth of the atmosphere
f	Coriolis parameter
g	Acceleration due to gravity
$\vec{k}$	Vertically directed unit vector
k	X-direction wave number
p	Pressure
p_o	Reference pressure
R	Gas constant for dry air
t	Time
T	Temperature
u	Velocity component in the x-direction
U	Mean wind velocity in the x-direction
v	Velocity component in the y-direction
$\vec{V}$	Horizontal wind vector
w	$\frac{dz}{dt}$, vertical velocity component in the z-coordinate system
x,y	Space coordinates
z	Height above sea level
z_s	Height of the lower boundary above sea level
Z	Distance from the upper boundary to the lower boundary
θ_o	Constant reference potential temperature
θ	Departure of the potential temperature from θ_o
θ_s	Mean θ as a function of z in the undisturbed atmosphere
$\varkappa$	R/c_p

Φ	$c_p \theta_o (p/p_o)^{\kappa} + gz$
ζ	$\frac{z - z_s}{D - z_s}$
$\dot{\zeta}$	$\frac{d\zeta}{dt}$, a measure of the vertical velocity component in the ζ-coordinate system
∇	Horizontal gradient operator
Δt	Finite difference in time
Δx	Mesh length in the x-direction
Δz	Finite difference in the vertical in the z-coordinate system
$\Delta \zeta$	Finite difference in the vertical in the ζ-coordinate system

ACKNOWLEDGEMENTS

The author wishes to express his sincere thanks and appreciation to Professor R. T. Williams for his patience, guidance and encouragement as thesis advisor. The author also wishes to thank Professor J. D. Mahlman for reading the manuscript and making several useful suggestions, Professors G. J. Haltiner and F. J. Winninghoff for their support and suggestions. Special thanks are extended to Captain J. R. Walton whose computer program was used as a basis for this study. The W. R. Church Computer Center of the Naval Postgraduate School provided time on its IBM 360 for the numerical integrations.

I. INTRODUCTION

The use of large scale numerical forecast models makes it necessary to introduce a topographical model of the surface of the earth for use in the lower boundary condition. Cressman [1960] notes that since the topography of the surface of the earth has many small scale features, it is necessary to smooth the topography when it is used as a boundary condition in a numerical forecast model. Mintz [1956] and Cressman [1960] indicate that the influence of small scale features of the topography can be included in a surface drag coefficient which varies from point to point.

One purpose of this study is to examine the validity of linear smoothing of the topography in numerical weather prediction. To accomplish this the flow over a small scale mountain was computed using a small grid mesh. The results of these computations were then smoothed. The mountain was then smoothed and the solution was recomputed. Since the parameters predicted in large-scale forecasts are interpreted as area averages, a comparison of the two results should show little, if any, difference if the smoothing technique is valid.

Mountain drag, or mountain torque, which arises from a difference in pressure on the two sides of a mountain, is important in the general circulation of the atmosphere. Studies of mountain drag associated with smaller scale mountains could be used to improve the calculation of the surface drag coefficient which was mentioned above. Miles [1968] showed that wave drag on an obstacle is a function of the height of the obstacle and of the mean flow perpendicular to the obstacle. The present paper investigates the effect of mountain height and initial static stability on mountain drag.

This study employes a two-dimensional, primitive equation model. The geostrophic current perpendicular to the mountain is constant. The mountain range is infinite in lateral extent which makes the model independent of y. A special coordinate system similar to that developed by Phillips [1957] was used. The equations were solved numerically with the use of a special finite difference scheme which was developed by A. Arakawa (see Langlois and Kwok, [1968]).

II. THE BASIC EQUATIONS

The basic equations used in this study are the Boussinesq equations. These equations will be applied to a model in which the flow is bounded above by a rigid horizontal plane. These equations neglect the compressibility of the atmosphere which, for this study, should not be of qualitative importance. It will be seen that the internal scale of the flow is small compared with the depth of the fluid. The hydrostatic approximation is made and heating and friction terms are neglected. The Boussinesq equations (Ogura and Phillips [1962]) may be expressed in the z-coordinate system as

$$\frac{\partial \vec{V}}{\partial t} + \vec{V}\cdot\nabla\vec{V} + w\frac{\partial \vec{V}}{\partial z} = -\nabla\Phi - f\vec{k}\times\vec{V}, \tag{1}$$

$$\frac{\partial \theta}{\partial t} + \vec{V}\cdot\nabla\theta + w\frac{\partial \theta}{\partial z} = 0, \tag{2}$$

$$\frac{\partial \Phi}{\partial z} = \frac{g}{\theta_o}\theta, \tag{3}$$

$$\nabla\cdot\vec{V} + \frac{\partial w}{\partial z} = 0 \tag{4}$$

where:

$$\theta = T(p_o/p)^{\varkappa} - \theta_o$$

In this model the only quantity which varies with latitude is Φ and it varies linearly. The Coriolis parameter is constant.

To simplify the finite differencing of the basic equations a modified coordinate system is introduced in which the lower boundary surface becomes a coordinate. This system makes it possible to introduce the effects of topography without employing uncentered horizontal space differences in the vicinity of the mountains. It also allows

application of the lower boundary condition at the actual surface of the mountain. In the proposed coordinate system the vertical advection terms are identically zero at both the upper and lower boundaries. This system of coordinates is very similar to the sigma system introduced by Phillips [1957].

The vertical coordinate, zeta, is defined as:

$$\zeta = \frac{z - z_s}{Z} \tag{5}$$

where:

$$Z = D - z_s$$

According to this definition $\zeta = 0$ at the lower boundary and $\zeta = 1$ at the upper boundary. Fig. 1 illustrates this coordinate system.

Transformation of equations (1) through (4) from the z-coordinate system into the ζ-coordinate system yields:

$$\frac{\partial \vec{V}}{\partial t} + \vec{V}\cdot\nabla\vec{V} + \dot{\zeta}\frac{\partial \vec{V}}{\partial \zeta} = -\nabla\Phi - \frac{\partial \Phi}{\partial \zeta}\left(\frac{\zeta - 1}{Z}\right)\nabla_h z_s - f\vec{k} \times \vec{V} \tag{6}$$

$$\frac{\partial \theta}{\partial t} + \vec{V}\cdot\nabla\theta + \dot{\zeta}\frac{\partial \theta}{\partial \zeta} = 0 \tag{7}$$

$$\frac{\partial \Phi}{\partial \zeta} = \frac{g}{\theta_o} Z\theta \tag{8}$$

$$\nabla\cdot Z\vec{V} + Z\frac{\partial \dot{\zeta}}{\partial \zeta} = 0 \tag{9}$$

In equations (6) through (9) ∇ is the horizontal gradient operator on zeta surfaces.

Since some of the following computations involve vertical averaging it is convenient to express the equations in flux form. Equations (6) through (9) in component form become:

$$\frac{\partial (M_x)}{\partial t} + \mathcal{L}(u) = -Z\frac{\partial \Phi}{\partial x} + \frac{g}{\theta_o} H\,(\zeta - 1)\frac{\partial Z}{\partial x} + fM_y \tag{10}$$

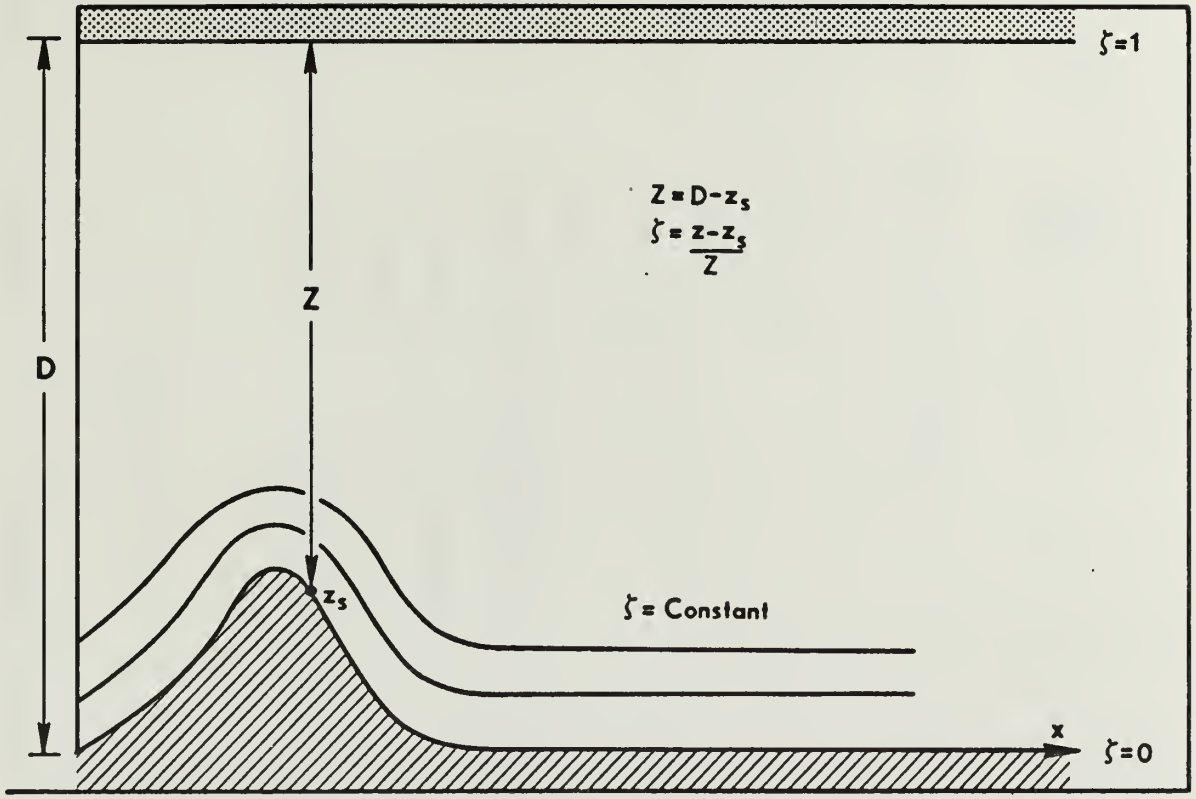

Figure 1. Schematic diagram of the zeta-coordinate system.

$$\frac{\partial(M_y)}{\partial t} + \mathcal{L}(v) = - Z \frac{\partial \Phi}{\partial y} - fM_x \tag{11}$$

$$\frac{\partial H}{\partial t} + \mathcal{L}(\theta) = 0 \tag{12}$$

$$\frac{\partial \Phi}{\partial \zeta} = \frac{g}{\theta_o} H \tag{13}$$

$$\frac{\partial(M_x)}{\partial x} + Z \frac{\partial \dot{\zeta}}{\partial \zeta} = 0 \tag{14}$$

where:

$$\mathcal{L}(s) = \frac{\partial}{\partial x}(sM_x) + \frac{\partial}{\partial \zeta}(\dot{\zeta} s Z)$$

$s = u, v, \theta$

and $M_x = uZ$, $M_y = vZ$, $H = \theta Z$.

The boundary conditions are:

$$\dot{\zeta} = 0 \text{ at } \zeta = 0, \text{ and} \tag{15}$$

$$\dot{\zeta} = 0 \text{ at } \zeta = 1. \tag{16}$$

For this study the flow will be independent of y and periodic in x. Since Φ is the only variable allowed to change in the y direction $\frac{\partial}{\partial y} = 0$ for all other variables.

To obtain an expression for Φ equation (13) may be integrated with respect to ζ,

$$\Phi = \int_0^{\zeta} \frac{g}{\theta_o} H \, d\zeta + C \tag{17}$$

The constant of integration, C, is eliminated by taking the vertical average of equation (17) and subtracting which gives the following expression for Φ:

$$\Phi = \frac{g}{\theta_o} \left(\int_0^{\zeta} H \, d\zeta - \overline{\int_0^{\zeta} H \, d\zeta} \right) + \overline{\Phi} \tag{18}$$

In the above equation and throughout the remainder of this paper $\overline{}^{\zeta}$ represents the vertical average of a given variable and $\overline{}$ represents the horizontal average.

Before a solution for Φ can be found, a value for $\overline{\Phi}^{\zeta}$ must be obtained. This is accomplished by first taking the vertical average of equation (10) thereby eliminating the vertical advection term. Next the vertically averaged equation is differentiated with respect to x yielding:

$$\frac{\partial^2}{\partial t \partial x}\overline{(M_x)}^{\zeta} + \frac{\partial^2}{\partial x^2}\overline{(M_x)}^{\zeta} = \frac{\partial}{\partial x}\left[-Z\frac{\partial \overline{\Phi}^{\zeta}}{\partial x} + \overline{\frac{\partial \Phi}{\partial \zeta}(\zeta-1)}\frac{\partial Z}{\partial x} + \overline{fM_y}^{\zeta}\right] \quad (19)$$

The first term of this equation is zero since the vertical average of equation (14) vanishes and the resulting equation is:

$$\frac{\partial}{\partial x}\left(Z\frac{\partial \overline{\Phi}^{\zeta}}{\partial x}\right) = \frac{\partial}{\partial x}\left[\frac{\partial}{\partial x}\overline{(M_x)}^{\zeta} + \overline{\frac{g}{\theta_o}H(\zeta-1)}\frac{\partial Z}{\partial x} + \overline{fM_y}^{\zeta}\right] \quad (20)$$

This equation can be solved diagnostically for $\overline{\Phi}^{\zeta}$.

To obtain $\frac{\partial \Phi}{\partial y}$ equation (18) is differentiated with respect to y yielding:

$$\frac{\partial \Phi}{\partial y} = \frac{g}{\theta_o}Z\left(\int_0^{\zeta}\frac{\partial \theta}{\partial y}\,d\zeta - \overline{\int_0^{\zeta}\frac{\partial \theta}{\partial y}\,d\zeta}\right) + \frac{\partial \overline{\Phi}^{\zeta}}{\partial y} \quad (21)$$

Since $\frac{\partial \theta}{\partial y} = 0$ for this study

$$\frac{\partial \Phi}{\partial y} = \frac{\partial \overline{\Phi}^{\zeta}}{\partial y} \quad (22)$$

and this quantity is assumed to be independent of x to keep the perturbations independent of y.

Now consider the domain averages of equations (10) and (11) which are:

$$\frac{d}{dt}\overline{(M_x)}^{\zeta} = -Z\frac{\partial \overline{\Phi}^{\zeta}}{\partial x} + \frac{g}{\theta_o}\overline{H(\zeta-1)}\frac{\partial Z}{\partial x} + \overline{fM_y}^{\zeta} \quad (23)$$

$$\frac{d}{dt}\overline{(M_y)} = -\overline{Z}\frac{\partial\overline{\Phi}}{\partial y} - \overline{fM_x} \tag{24}$$

Initially $\frac{\partial\overline{\Phi}}{\partial y}$ is computed geostrophically as follows:

$$\frac{\partial\overline{\Phi}}{\partial y} = -\frac{f}{\overline{Z}}\overline{(M_x)}_{t=0} \tag{25}$$

If this relation is used for all time and if the mass flux in the y direction is zero initially, then $\overline{M_y}$ will be zero for all time. The first two terms on the right side of equation (23) represent the mountain drag. The sum of these two terms was shown by computation to be negative in the mean as expected from physical considerations. This will lead to a continual loss of x-momentum. A loss such as this would make a quasi-steady final state impossible. An artificial source of momentum is thus required in this simple model to maintain the mean zonal flow. The artificial source of momentum is provided by holding $\frac{\partial\overline{\Phi}}{\partial y}$, as obtained in equation (25), constant for all time. In this case if $\overline{M_x}$ is decreased below the initial geostrophic value $\overline{M_y}$ will increase and restore the momentum loss. Thus, in the long term mean, the mountain terms are balanced by the mean Coriolis force due to a net y-momentum flux.

III. FINITE DIFFERENCE EQUATIONS

Equations (10) through (14), and (18) are solved by introducing finite differences in x, ζ, and t. The space finite differences employ a variation of a scheme developed by Arakawa [1966] (see also Lilly [1965]). The basic scheme was designed to conserve total energy in addition to conserving the squares of u, v, and θ with respect to the advection terms. This scheme was also designed to avoid the non-linear computational instability which was discovered by Phillips [1959].

The time differencing scheme employs a variation of the Matsuno [1966] two stage differencing scheme which is also referred to as the Euler simulated backward time step differencing scheme. This scheme is similar to that used in the general circulation model developed by A. Arakawa (see Langlois and Kwok [1968]). The modification makes it possible to avoid a checkerboard spatial pattern by alternating between centered and uncentered space differences in certain terms.

The Euler backward difference scheme may be written in the following form

$$s^* = s^t + \Delta t F^t \qquad \text{(step 1)}$$

$$s^{t+1} = s^t + \Delta t F^* \qquad \text{(step 2)}$$

where

s = u, v, θ and

F is the right hand side minus the linear operator $\mathfrak{L}(u)$ as defined by equations (10) through (12).

Centered space differences are employed to compute F^t in step 1 above and uncentered space differences, using the values of s* obtained in step 1, are used to compute F* in step 2. During computation, forward

spatial differences are used for even time steps and backward spatial differences are used for odd time steps. This method allows geostrophic adjustment to occur at the smallest scale recognized by the model.

The vertical domain is divided into 18 layers such that $\Delta\zeta = 1/18$ for each layer. The boundary surfaces are denoted by the subscript i, where i = 1 at the lower boundary, the surface, to i = 19 at the top of the model. The quantities M_x, M_y, H, and Φ are computed on the even levels and $\dot{\zeta}$ is computed on the odd levels. Throughout the remainder of this study j denotes the horizontal grid index with Δx as the grid mesh length. For the remainder of this paper CDF, FDF and BDF will represent centered difference form, forward difference form and backward difference form, respectively.

The finite difference form of the linear operator (s), where is is any dependent variable, can be written

$$\mathfrak{L}(s)_{i,j} = \frac{\left[(s_{i,j+1} + s_{i,j})\,(M_{x+}) - (s_{i,j} + s_{i,j-1})\,(M_{x-})\right]}{2\Delta x} + \frac{Z_j\left[(\dot{\zeta}_{i+1,j}\, s_{i+1,j}) - (\dot{\zeta}_{i-1,j}\, s_{i-1,j})\right]}{2\Delta\zeta} \qquad (26)$$

In equation (26) the flux forms M_{x+} and M_{x-} are defined as:

$$M_{x+} = \frac{(M_{x\ i,j+1} + M_{x\ i,j})}{2} \quad \text{and}$$

$$M_{x-} = \frac{(M_{x\ i,j} + M_{x\ i,j-1})}{2} \quad \text{(CDF)}$$

$$M_{x+} = M_{x\ i,j+1} \quad \text{and}$$

$$M_{x-} = M_{x\ i,j} \quad \text{(FDF) and}$$

$$M_{x+} = M_{x\ i,j} \quad \text{and}$$

$$M_{x-} = M_{x\ i,j-1} \quad \text{(BDF)}$$

The finite difference approximation to the integral in equation (17) is:

$$\int_0^{\zeta_k} H \, d\zeta = \sum_{i=1}^{i=k-2} (H_{i+2,j} + H_{i,j}) \, \Delta\zeta + C, \; k \geq 3 \tag{27}$$

The value of the constant of integration, C, is not important since it will vanish when the vertical average of equation (27) is taken.

When i is odd, equation (13) can be approximated with:

$$\Phi_{i+1,j} = \Phi_{i-1,j} + 2\Delta\zeta \left(\frac{g}{\theta_o}\right) H_{i,j} \tag{28}$$

The continuity equation, equation (14), can be approximated with:

$$\dot{\zeta}_{i+1,j} = \dot{\zeta}_{i-1,j} + \frac{1}{Z_j} \frac{2\Delta\zeta}{\Delta x} (M_{x+} - M_{x-}) \tag{29}$$

The flux forms M_{x+} and M_{x-} are as defined above.

Since all of the dependent variables occur at each grid point, the x derivatives are approximated by:

$$\left(\frac{\partial s}{\partial x}\right)_{i,j} = \frac{\delta s}{\Delta x} \tag{30}$$

The form of the dependent variable δs is defined as:

$$\delta s = \frac{(s_{i,j+1} - s_{i,j-1})}{2} \text{ (CDF)}$$

$$\delta s = (s_{i,j+1} - s_{i,j}) \text{ (FDF) and}$$

$$\delta s = (s_{i,j} - s_{i,j-1}) \text{ (BDF)}$$

To maintain consistency within the model the finite difference form of equation (20) is obtained from the finite difference form of equation (12) and appears in the following form:

$$A_j \overline{\Phi}_{j+1} - B_j \overline{\Phi}_j + C_j \overline{\Phi}_{j-1} = - \frac{\delta D}{\Delta x} \qquad (31)$$

where:

$$B_j = A_j + C_j$$

$A_j = Z_{j+1}$ and $C_j = Z_{j-1}$ (used with CDF)

$A_j = Z_j$ and $C_j = Z_{j-1}$ (used with FDF)

$A_j = Z_{j+1}$ and $C_j = Z_j$ (used with BDF) and

$$D_j = \frac{1}{\Delta x} \left(\overline{\frac{u_{i,j+1} + u_{i,j}}{2} M_{x+}} - \overline{\frac{u_{i,j} + u_{i,j-1}}{2} M_{x-}} \right)$$

$$+ \frac{g}{\theta_o} \overline{H_{i,j}} \frac{\delta Z}{\Delta x} + \overline{fM_y}_{i,j}$$

where:

$$\delta D = \frac{(D_{j+1} - D_{j-1})}{2}$$ (used with CDF)

$\delta D = D_j - D_{j-1}$ (used with FDF), and

$\delta D = D_{j+1} - D_j$ (used with BDF)

In the above equations M_{x+}, M_{x-}, and δs are as defined above.

A solution for $\overline{\Phi}$ can now be obtained using the exact technique described on page 198 of Richtmyer and Morton [1967].

IV. SCALE ANALYSIS

The following scale analysis is done in the z-coordinate system as a matter of convenience. The analysis will be useful in determining the initial conditions for this model and will serve as an aid in the interpretation of the numerical solutions.

The following non-dimensional independent variables are defined:

$$x' = \frac{x}{L} \text{ and} \tag{32}$$

$$z' = \frac{z}{d} \tag{33}$$

L and d are the horizontal and vertical scales of the disturbance. They are due to the characteristics of the mountain and other physical parameters.

$$u = U + \mathcal{R}_o\, Uu' \tag{34}$$

$$v = \mathcal{R}_o\, Lfv' \tag{35}$$

$$w = UB\,\frac{w'}{L} \tag{36}$$

$$\theta = \theta_s + B\,\frac{\partial \theta_s}{\partial z}\,\theta' \tag{37}$$

$$\Phi = \frac{g}{\theta_o}\int \theta_s\, dz + Bd\,\frac{g}{\theta_o}\,\frac{\partial \theta_s}{\partial z}\,\Phi' \tag{38}$$

The constant, U, represents the zonal flow away from the mountain. The quantity $\frac{\partial \theta_s}{\partial z}$, represents the stratification of the basic undisturbed atmosphere which, for this study, is assumed to be constant. The scale of the meridional component of the wind is:

$$V = \frac{LfB}{d} \tag{39}$$

Two dimensionless numbers appear in the analysis. They are:

$$R_o = \frac{U}{fL} \quad \text{and} \tag{40}$$

$$\mathcal{R}_o = \frac{V}{fL} = \frac{B}{d} \tag{41}$$

R_o is the Rossby number based on the zonal wind and the mountain scale. $\mathcal{R}_o$ is the disturbance Rossby number and is so called because it is based on the amplitude of the v component of the wind.

The scale analysis requires that:

$$d = Lf\left(\frac{g}{\theta_o}\frac{\partial \theta_s}{\partial z}\right)^{-1/2} \tag{42}$$

as long as $d < D$.

Using the above definitions the steady state non-dimensional equations may be written:

$$R_o^2\left(\frac{\partial u'}{\partial x'} + \mathcal{R}_o\left(u'\frac{\partial u'}{\partial x'} + w'\frac{\partial u'}{\partial z'}\right)\right) = -\frac{\partial \Phi'}{\partial x'} + v' \tag{43}$$

$$\frac{\partial v'}{\partial x'} + \mathcal{R}_o\left(u'\frac{\partial v'}{\partial x'} + w'\frac{\partial v'}{\partial z'}\right) = -u' \tag{44}$$

$$\frac{\partial \theta'}{\partial x'} + w' + \mathcal{R}_o\left(u'\frac{\partial \theta'}{\partial x'} + w'\frac{\partial \theta'}{\partial z'}\right) = 0 \tag{45}$$

$$\frac{\partial u'}{\partial x'} + \frac{\partial w'}{\partial z'} = 0 \tag{46}$$

$$\frac{\partial \Phi'}{\partial z'} = \theta' \tag{47}$$

The boundary conditions to be applied are:

$$w' = \frac{\partial z'}{\partial x'} \text{ at } z = z_s \quad \text{and} \tag{48}$$

$$w' = 0 \text{ at } z' = \frac{D}{d} \tag{49}$$

This scaling is consistent with the numerical solutions which will be presented later. Note that if the R_o^2 and $\mathcal{R}_o$ terms are eliminated, the quasi-geostrophic equations result. If just the R_o^2 term is dropped, the balance equations as given by Charney [1962] result.

V. INITIAL CONDITIONS

The profile of the mountain used in this study is given by the cosine squared of the horizontal distance. The mountain is 1200 km wide, has an amplitude designated B and is duplicated every 6000 km. The lower boundary of the model is flat and horizontal except where the mountain exists.

The initial state is derived from the steady state, quasi-geostrophic equations which were shown to be linear in the preceding section. These equations are:

$$v' = \frac{\partial \Phi'}{\partial x'} \tag{50}$$

$$u' = -\frac{\partial v'}{\partial x'} \tag{51}$$

$$\frac{\partial \theta'}{\partial x'} + w' = 0 \tag{52}$$

$$\frac{\partial u'}{\partial x'} + \frac{\partial w'}{\partial z'} = 0 \tag{53}$$

$$\frac{\partial \Phi'}{\partial z'} = \theta' \tag{54}$$

The equation necessary to obtain the initial fields of u, v, and θ is the potential vorticity equation for this set of linearized equations. To obtain the potential vorticity equation, differentiate equations (51) and (52) with respect to x. Subtract equation (53) from the differentiated form of equation (52). The resulting equation is:

$$\frac{\partial}{\partial z'}\left(\frac{\partial \theta'}{\partial x'}\right) - \frac{\partial u'}{\partial x'} = 0 \tag{55}$$

Now differentiate equations (51) and (52) with respect to x and equation (54) with respect to z and substitute into equation (55). The resulting equation is the potential vorticity equation:

$$\frac{\partial}{\partial x'}\left(\frac{\partial^2 \Phi'}{\partial z'^2} + \frac{\partial^2 \Phi'}{\partial x'^2}\right) = 0 \tag{56}$$

To obtain the initial solution for this study the following boundary conditions are applied:

$$\frac{\partial \Phi'}{\partial z'} = 0 \text{ at } z' = \frac{D}{d} \text{ and} \tag{57}$$

$$\frac{\partial \Phi'}{\partial z'} = z_s \text{ at } z = 0 \tag{58}$$

Equation (56) is satisfied if:

$$\frac{\partial^2 \Phi'}{\partial z'^2} + \frac{\partial^2 \Phi'}{\partial x'^2} = 0 \tag{58}$$

A general solution of equation (58), here $x' = kx$, is:

$$\Phi'(x',z') = F(z') \cos x' \tag{59}$$

Applying this solution to equation (58) at the upper boundary and solving for F(z') yields:

$$F(z') = A \cosh\left(z' - \frac{D}{d}\right) \tag{60}$$

From this it follows that:

$$\Phi'(x',z') = A \cos x' \cosh\left(z' - \frac{D}{d}\right) \tag{61}$$

The mountain topography can be Fourier analyzed into a cosine series. Each component of that series will have the following form if x is non-dimensionalized with the wave number of the component.

$$z'_s = B' \cos x' \tag{62}$$

When the solution for this component is obtained, the quantities can be dimensionalized and summed to satisfy the complete boundary condition.

Differentiation of equation (61) with respect to z' and evaluation of the resulting equation at $z' = z'_s$ gives the following result:

$$\left(\frac{\partial \Phi'}{\partial z'}\right)_{z'=z_s} = A \cos x' \sinh\left(z'_s - \frac{D}{d}\right) \tag{63}$$

If it is assumed for this analysis that z'_s is sufficiently small that equation (63) can be applied at $z'_s = 0$, then this equation can be solved for A:

$$A = -\frac{1}{\sinh\left(\frac{D}{d}\right)} \tag{64}$$

The final solution for Φ' is:

$$\Phi' = \frac{1}{\sinh\left(\frac{D}{d}\right)} \cos x' \cosh\left(z' - \frac{D}{d}\right) \tag{65}$$

From this solution for Φ' follow the solutions for u', v', and θ':

$$v' = -\frac{1}{\sinh\left(\frac{D}{d}\right)} \sin x' \cosh\left(z' - \frac{D}{d}\right) \tag{66}$$

$$u' = \frac{1}{\sinh\left(\frac{D}{d}\right)} \cos x' \cosh\left(z' - \frac{D}{d}\right) \tag{67}$$

$$\theta' = \frac{1}{\sinh\left(\frac{D}{d}\right)} \cos x' \sinh\left(z' - \frac{D}{d}\right) \tag{68}$$

A Fourier series of the full lower surface yields:

$$z_s = \sum_k B(k) \cos kx$$

in dimensional form. Solutions (66) through (68), when dimensionalized, can be summed to give the following initial conditions:

$$u = U + \sum_{k=1}^{nw} \frac{k^2 \, UB(k) \, \frac{g}{\theta_o} \frac{\partial \theta_s}{\partial z}}{f^2 \, \alpha \sinh(\alpha D)} \cosh[\alpha(z-D)] \cos(kx) \qquad (69)$$

$$v = \sum_{k=1}^{nw} \frac{k \, B(k) \, \frac{g}{\theta_o} \frac{\partial \theta_s}{\partial z}}{f \sinh(\alpha D)} \cosh[\alpha(z-D)] \sin(kx) \qquad (70)$$

$$\theta = \theta_s + \sum_{k=1}^{nw} \frac{B(k) \frac{\partial \theta_s}{\partial z}}{\sinh(\alpha D)} \sinh[\alpha(z-D)] \cos(kx), \text{ and} \qquad (71)$$

$$B(k) = \frac{\frac{B}{\pi} \sin\left(\frac{nw \; npm \; \pi}{np}\right)}{nw\left[1 - \left(\frac{npm \; k}{np}\right)^2\right]} \qquad (72)$$

where:

$$\alpha \equiv \frac{k}{f}\left(\frac{g}{\theta_o} \frac{\partial \theta_s}{\partial z}\right)^{1/2} \quad \text{and}$$

nw is the number of wave numbers used, npm is the number of points in the mountain and np is the total number of horizontal grid points in the model.

The first 20 wave numbers were used to initialize the wind and temperature fields. Any number up to and including 20 could have been used with k = 20 yielding the smoothest initial solution. Any number greater than 20 would have introduced aliasing since the waves generated would have a wave length less than two grid lengths.

In the initial fields the constants used were U = 8 m sec^{-1}, $\frac{\partial \theta_s}{\partial z}$ = 4.0 $^oK \; km^{-1}$, D = 9 km, $\frac{g}{\theta_o}$ = 0.0327 m sec^{-2} $(^oK)^{-1}$, and f = 10^{-4} sec^{-1}. The value of θ_s was computed for each point from the relation:

$$\theta_s = \frac{\partial \theta_s}{\partial z}\left[\frac{D}{2} + Z \; (\zeta - 1)\right]$$

VI. RESULTS

In this study Δx = 150 km, Δt = 20 min, and nine equally spaced levels in zeta were used. Seven values of B with $\frac{\partial \theta_s}{\partial z} = 4\ ^{o}K\ km^{-1}$ and eleven values of $\frac{\partial \theta_s}{\partial z}$ at B = 1575 m were employed.

Values of the mountain height were computed using the function $B \cos^2 (kx)$. This function provides a smooth profile at the base of the mountain. First, solutions were computed using this function to determine the mountain profile. The solutions were then computed using a linearly smoothed mountain profile. The smoothing was accomplished by applying the following linear formula:

$$Z_j^{\nu+1} = \left(\frac{Z_{j+1} + Z_j + Z_{j-1}}{3}\right)^{\nu} \tag{73}$$

This procedure was repeated four times. The resulting mountain height was about two thirds that of the original mountain height and the horizontal extent was approximately doubled. In each case the solutions were allowed to converge toward a quasi-steady state. To permit comparison of the various cases the results were converted from the zeta-surfaces to the z-surfaces at one km intervals. In this study R_o is independent of the mountain height and its value is R_o = .419.

The general features of the flow were basically the same for all cases and were similar to those reported by Walton [1968]. There was a ridge in the pressure field over the mountain. The v component of the wind was from the south on the windward side of the mountain and from the north on the leeward side. The u component of the wind was at a maximum near the surface over the mountain and decreased rapidly with height to a minimum at the top of the atmosphere. Over the plain,

away from the mountain, the u component was a minimum near the surface and increased very slightly with height to a maximum at the top of the atmosphere. The potential temperature was a minimum over the mountain crest.

Fig. 2 is a graph of the difference between the maximum value of Φ in the ridge and the minimum value of Φ at the bottom of the trough, at the three km level, with respect to mountain height. The upper curve represents the smoothed solutions from the unsmoothed mountain.

The difference between the smoothed and unsmoothed solutions is least for mountain heights less than 900 m. Below this height the solutions are almost identical. The scale analysis of the basic equations used in this study showed that when R_o^2 is small the balance approximation should hold. When $\mathcal{R}_o$ is also small the equations reduce to the linear quasi-geostrophic equations. Since the equations are linear for $\mathcal{R}_o$ small the solutions should be nearly equal in this range as they actually are. At mountain heights greater than 900 m the non-linear effects become large enough to cause a marked separation of the two curves. These results are comparable in magnitude to those obtained by Walton [1968]. In his study he applied a different differencing scheme to obtain solutions to this same model.

The addition of the artificial source of momentum suggested in Section II appears to have been valid. The slow decay in mean zonal velocity with time noted by Walton [1968] did not occur. In providing the artificial source of momentum it was assumed that the model would come into adjustment and that the mountain drag term would be balanced by the term denoting mass flux in the y-direction. Fig. 3 shows a plot of these two quantities versus time. This figure shows the values for a

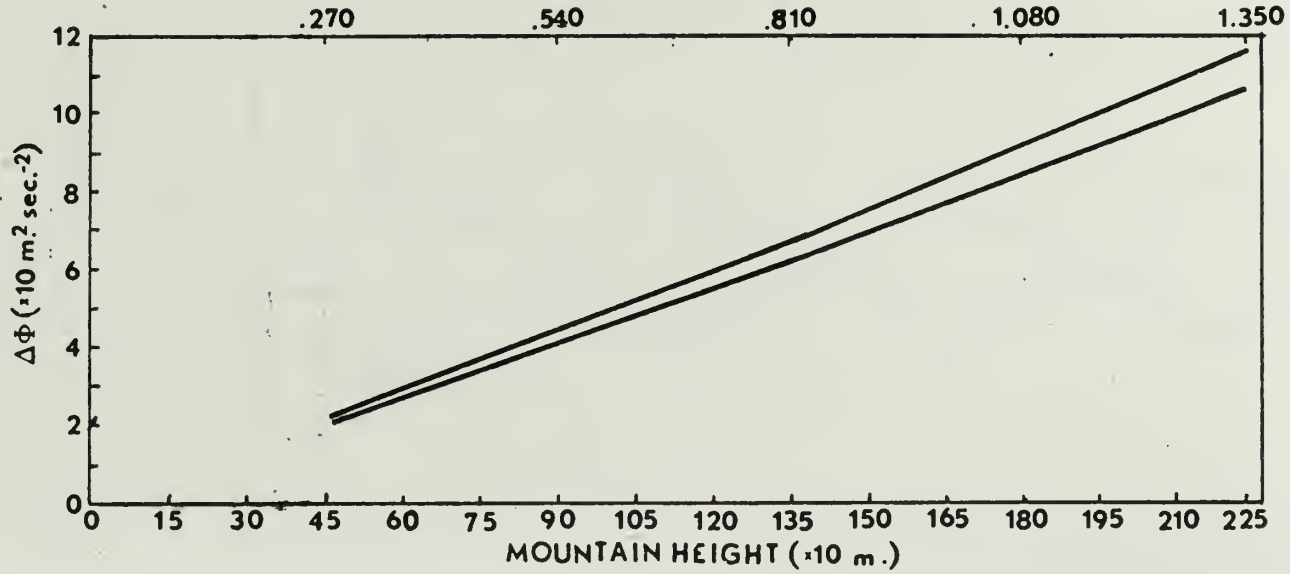

Figure 2. Graph of $\Delta\Phi$ versus time. $\Delta\Phi$ is the difference between the maximum Φ over the mountain and the minimum Φ over the plain at the three km level. The upper curve represents the smoothed solution for the unsmoothed mountain and the lower curve represents the solution for the smoothed mountain.

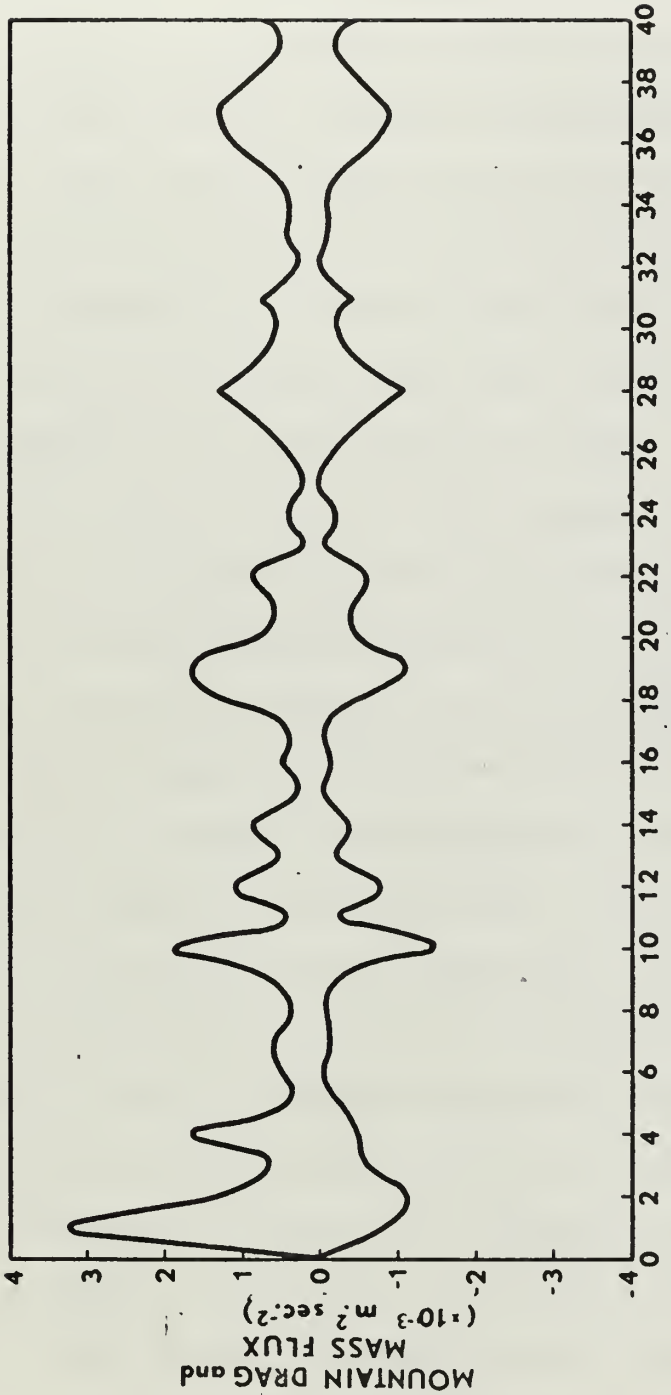

Figure 3. Plot of y-direction mass flux and mountain drag with respect to time. Y-direction mass flux is the upper curve and mountain drag is the lower curve.

single mountain height, however it is representative of all the mountain heights in this study. The upper curve represents the momentum flux in the y-direction and the lower curve represents the mountain drag. It can be seen that these two quantities do behave as expected after the initial period when the model is coming into adjustment. It should be noted that the sum of the two curves does not equal zero. The long term change in the x-mass flux is very small. The reason for this difference is apparently due to the fact that centered space differences were used to calculate the mountain drag while uncentered differences were used to calculate the actual forecast variables.

The solutions, represented by $\Delta\Phi$, did not appear to be converging significantly at the end of 40 days into the forecast period. For the higher values of mountain height there appeared to be slight convergence, however this may have been due to the time finite differencing scheme which tends to damp the computational mode of solution. Fig. 4 is an example of the oscillation of the solution obtained. These oscillations have a period of about eight days. This pattern was identical for all cases with only the amplitude of oscillation varying. The amplitude increased with increasing mountain height. This oscillation appears to be the result of mechanical interaction between the mountains. One case involving a mountain height of 2025 m was computed retaining the width of the mountain at 1200 km but doubling the width of the plain from 4800 km to 9600 km. As a result of this the number of oscillations occurring in a 40 day forecast was diminished by one half with the amplitude of oscillation decreasing slightly. The values used in Fig. 2 are the mean values, at a given height, about which $\Delta\Phi$ oscillated.

As a check of the validity of the geostrophic assumption the v component of the geostrophic wind was computed. Except in the near vicinity

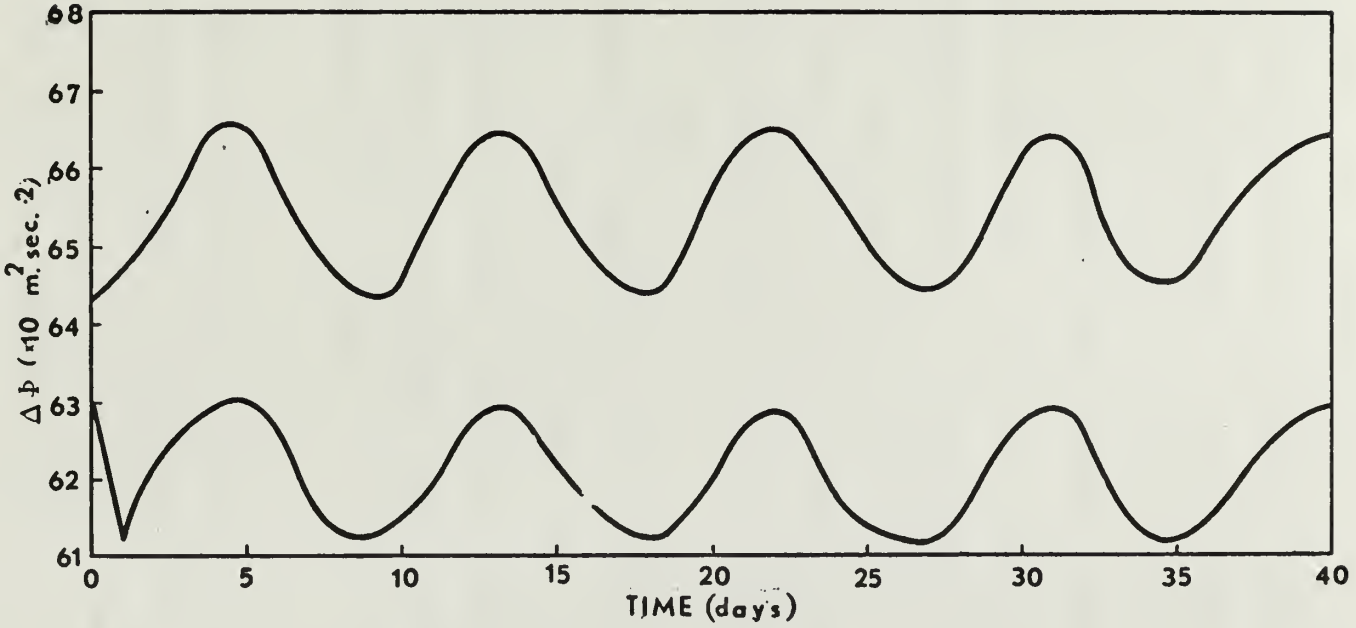

Figure 4. Graph of the time variation of $\Delta\Phi$. Results apply to the 1350 m mountain at the three km level.

of the mountain the values obtained from the forecast equations and the values obtained from the geostrophic computations were similar. The difference between the geostrophic and actual v component was less than ten percent in conformity with equation (13).

The variation of mountain drag with mountain height and with static stability was also investigated. Fig. 5 displays the results of the variation of mountain drag with mountain height. From this figure it can be seen that mountain drag increases quadratically with increasing mountain height. Fig. 6 shows the relationship between mountain drag and static stability. This figure shows that mountain drag increases linearly with increasing static stability. An investigation of the gross features of the flow for increasing static stability at a constant mountain height showed no significant changes except in magnitude.

The stream function was computed and streamlines were drawn for each mountain height at selected time spacing. Fig. 7 is a typical example of the streamlines obtained. It shows horizontal flow over the plain at all levels and flow conforming to the mountain in the vicinity of the mountain with the upper level flow nearly horizontal everywhere.

In the case where B = 2250 m static instability developed about 36 hours into the forecast period. A comparison of the u and Φ fields obtained in the hydraulic jump case B described by Houghton and Kasahara [1968] with those obtained in this study for B = 2250 m shows a marked similarity in the structure of the fields. Houghton and Kasahara used a single layer, non-rotating model. The lower values of mountain height used in the present study apparently fall into the

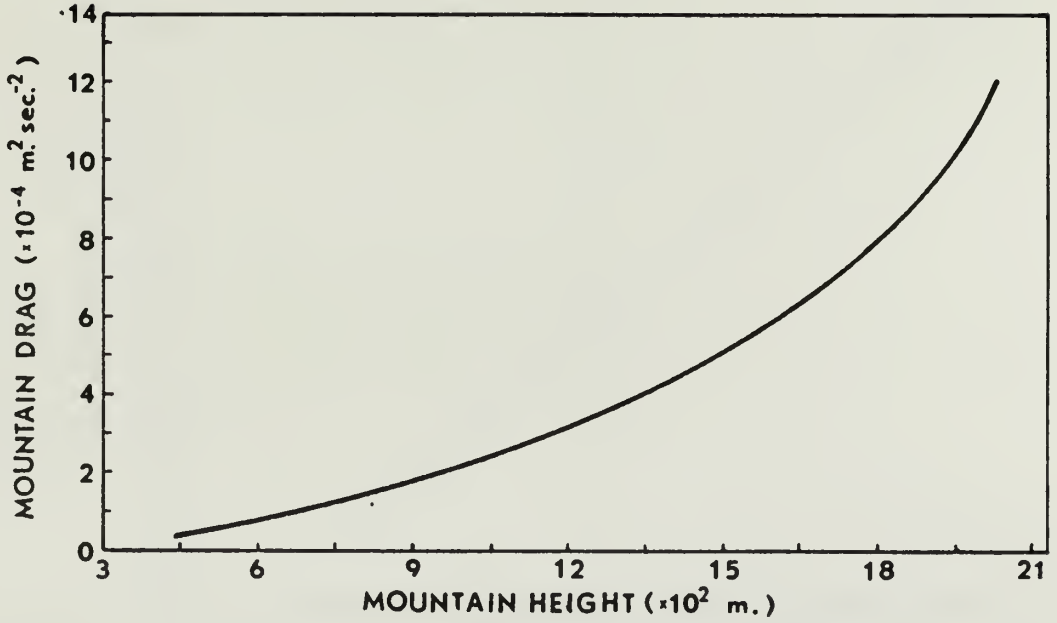

Figure 5. Variation of mountain drag with mountain height.

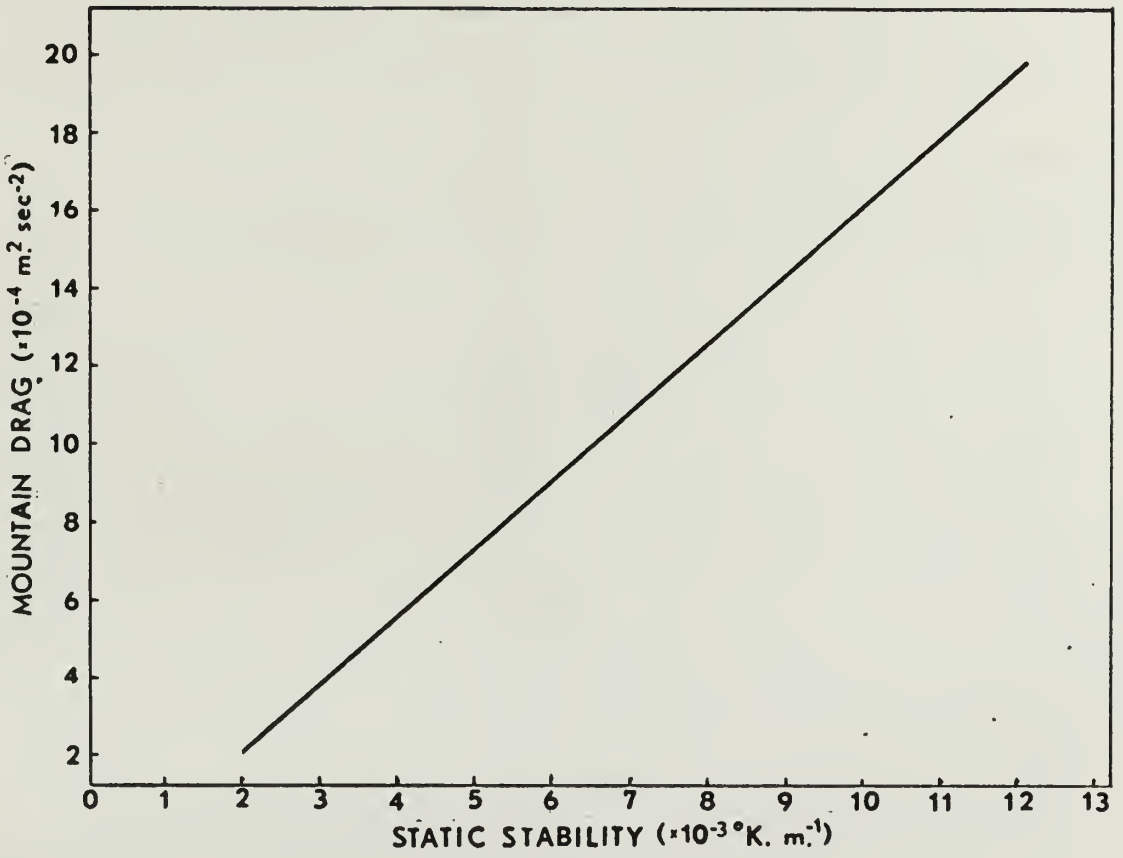

Figure 6. Variation of mountain drag with static stability.

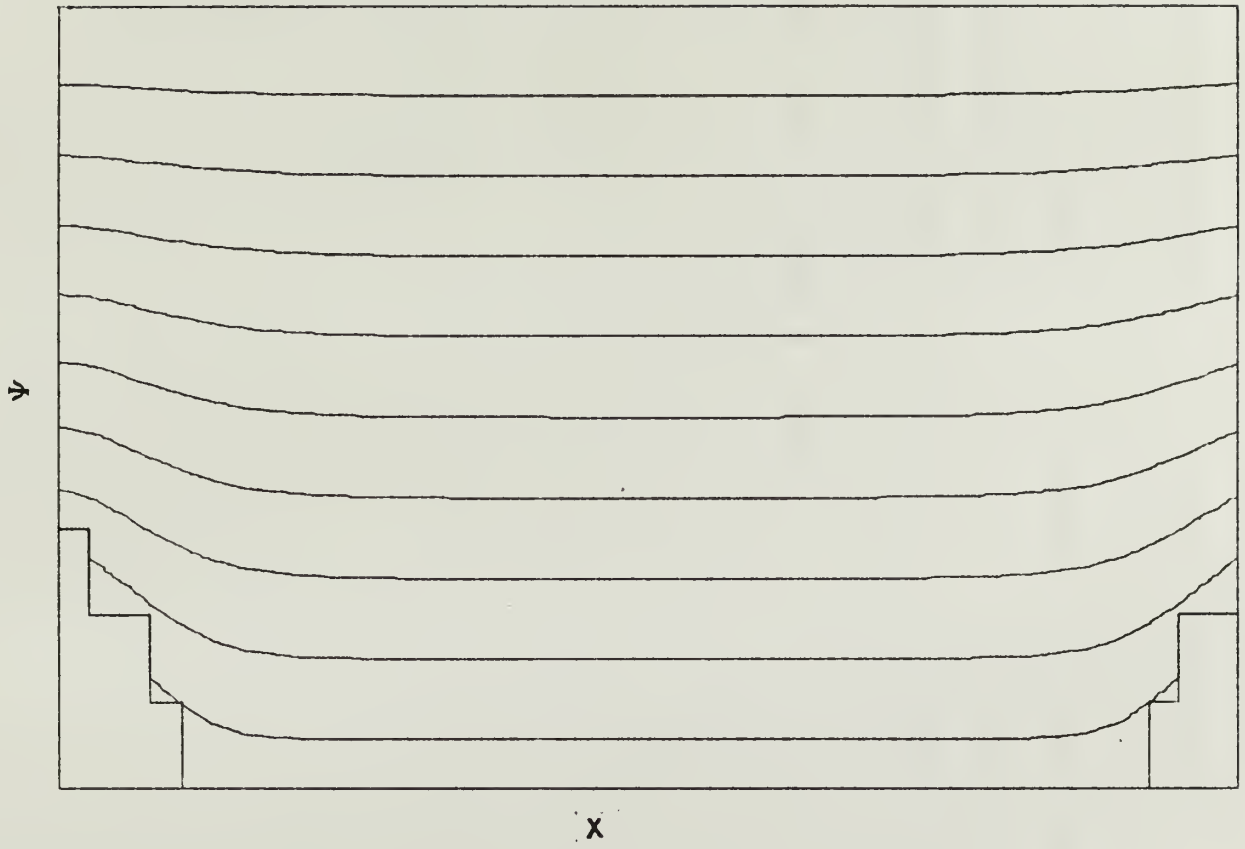

Figure 7. Typical streamlines.

non-critical, or no jump domain, described by Houghton and Kasahara. As mountain height increases the values eventually fall in the hydraulic jump domain. The reason for the static instability at B = 2250 m is thus attributed to hydraulic jump. Fig. 8 shows the values of u initially and six hours later for B = 2250 m at the three km level. The development of the minimum in u in the lee of the mountain is already evident even though static instability has not yet occurred. This model is not appropriate for the treatment of hydraulic jump because of approximations which have been made. Calculations of mountain drag were not made for this case but it is expected that if these calculations had been made the character of the drag properties would have been modified above B = 2025 m.

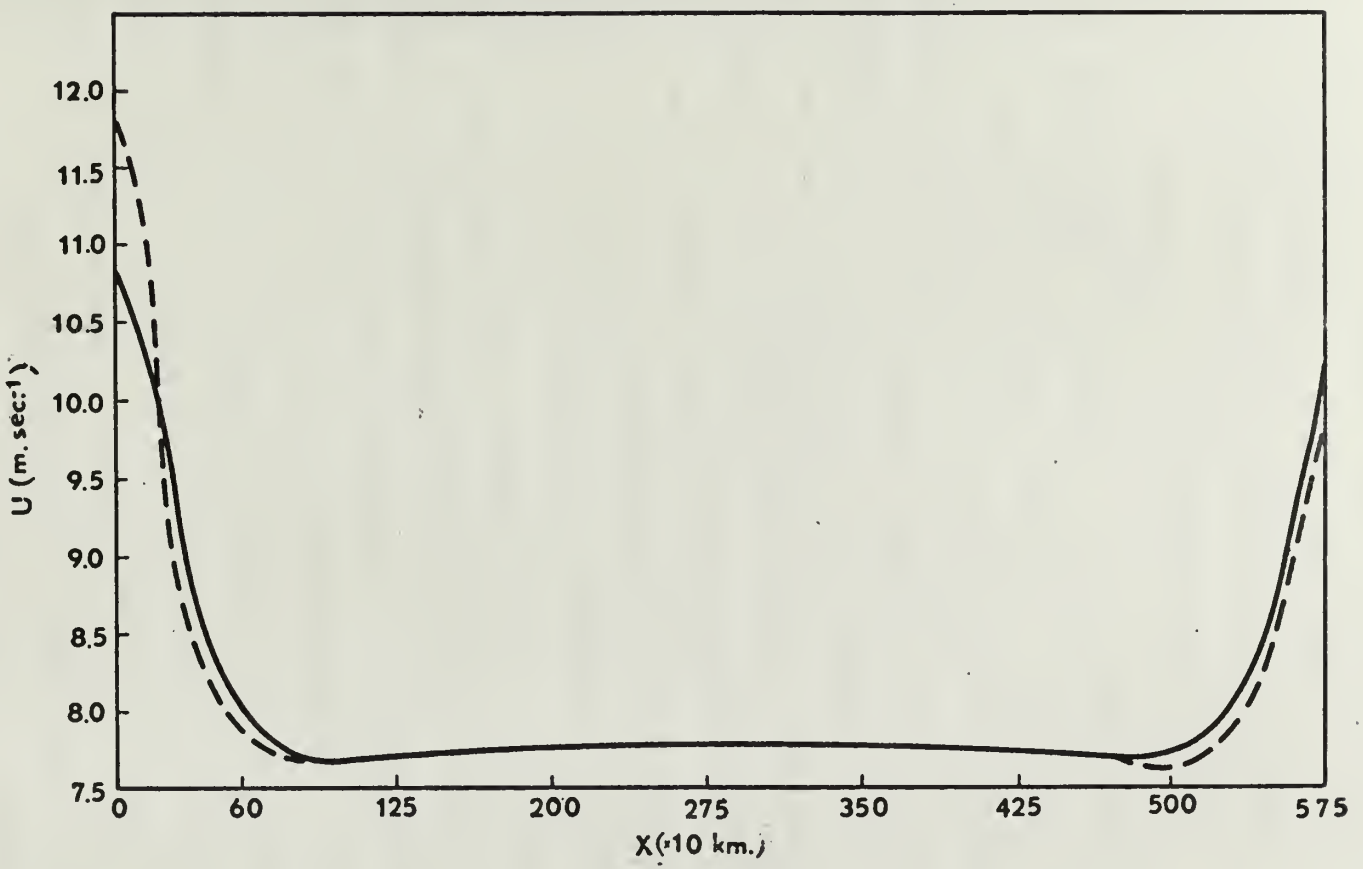

Figure 8. U component of the wind at t = 0 and at t = 6 hours for B = 2250 m at the three km level. The solid curve represents u at t = 0 and the dashed curve represents u at t = 6 hours.

VII. CONCLUSIONS

Since this study involved only one horizontal scale, only one value of the Rossby number ($R_o = U/fL$) was considered. Solutions obtained in this study showed that linear smoothing of the topography an error which increases as the disturbance Rossby Number $\left[\mathcal{R}_o = \frac{B}{d} = \frac{B}{fL}\left(\frac{g}{\theta_o}\frac{\partial\theta_s}{\partial z}\right)^{1/2}\right]$ increases. If the results from this study could be extrapolated to smaller scales, i.e., where $\mathcal{R}_o$ is larger, the difference between results obtained using a smoothed topography and those obtained using an unsmoothed topography would be even greater. This is consistent with the example given by Charney [1967] in which he considered an infinitesimally thin mountain, oriented along a meridian and extending to the top of the atmosphere. Without smoothing it would act as an absolute barrier, however, with smoothing its vertical extent would be decreased to nothing and it would have no effect on atmospheric flow. However it is not clear what error will be found if $\mathcal{R}_o$ becomes large enough for pressure jumps to form. The error behavior will probably be different than that obtained here.

The addition of an artificial source of momentum did maintain the mean value of the u component of the flow at a value near the initial mean zonal flow. A comparison of the values of $\mathcal{R}_o$ obtained in this study and those obtained by Walton [1968] did not show any significant difference in the results obtained for smooth and unsmoothed mountains.

By doubling the size of the plain between the mountains it was observed that the period of oscillation of the $\Delta\Phi$ field was reduced by one half. It was thus concluded that this oscillation is due, at least in part, to mechanical interactions between the mountains.

Mountain drag computed for varying mountain heights at a constant static stability showed an apparent quadratic relationship between increasing drag and increasing mountain height. Mountain drag computed for varying static stability at a constant mountain height showed an apparent linear relationship between increasing drag and increasing stability.

For the case when B = 2250 m static instability resulted early in the forecast period. The reason for this instability was attributed to the formation of a hydraulic jump. This cannot be definitely stated as the model, in the form which was used for this study, was not appropriate for the treatment of hydraulic jump because of the lack of friction and because of certain approximations which had been made.

Further studies with this model should be conducted using a wider range of mountain scales. This would give a more complete relationship between mountain drag and mountain structure which could be used in parameterizing mountain effects in numerical weather prediction models. The drag could be obtained for the larger values of $\mathcal{R}_o$ if appropriate treatment of the hydraulic jump is included. The mechanical interaction between the periodic mountains could be reduced if a variable mesh length grid in the horizontal scale of the model is used. This would permit a short mesh length in the vicinity of the mountain where most of the activity is.

LIST OF REFERENCES

Arakawa, A., 1966: Computational design for long-term numerical integration of the equation of fluid motion: Two-dimensional incompressible flow. Part 1. J. Comput. Phys., 1, 119-143.

Charney, J. G., 1962: Integration of the primitive and balance equations. Proc. Intern. Symp. Numerical Weather Prediction, Tokyo, 61-152.

Charney, J. G., 1967: Some remaining problems in numerical weather prediction. Advances in Numerical Weather Prediction, The Travelers Research Center, Inc., Hartford, Conn., 61-70.

Cressman, G. P., 1960: Improved terrain effects in barotropic forecasts. Mon. Wea. Rev., 88, 327-342.

Houghton, D. H. and Kasahara, A., 1968: Non-linear shallow fluid flow over an isolated ridge. Comm. Pure Appl. Math., 21, 1-23.

Langlois, W. E. and Kwok, H. C. W., 1968: Numerical simulation of weather and climate, Part I. Physical Description of the Model. Large Scale Scientific Computations Dept., IBM Research Laboratory, San Jose, Calif., 95 pp.

Lilly, D. K., 1965: On the computational stability of numerical solutions of time-dependent non-linear geophysical fluid dynamics problems. Mon. Wea. Rev., 93, 11-26.

Matsuno, T., 1966: Numerical integration of the primitive equations by a simulated backward difference method. J. Met. Soc. Japan, 44, 76-84.

Miles, J. W., 1968: Waves and wave drag in stratified flows, Appl. Mech., Proc. Twelfth Intern. Cong. Appl. Mech., Stanford Univ., 50-76.

Mintz, Y., 1956: An empirical determination of the surface drag coefficients for extended range and long-range numerical weather forecasting and the study of the general circulation. Scientific Report No. 3, Contract AF 19(604)-1282, University of Calif., Los Angeles, Dept. of Meteorology, 18 pp.

Ogura, Y. and Phillips, N. A., 1962: Scale analyses of deep or shallow convection in the atmosphere. J. Atmos. Sci., 19, 173-179.

Phillips, N. A., 1957: A coordinate system having some special advantages for numerical forecasting. J. Meteor., 14, 184-185.

Phillips, N. A., 1959: An example of non-linear computational instability. The Atmosphere and the Sea in Motion (edited by B. Bolin) Rockefeller Institute Press in association with the Oxford University Press, New York, pp. 501-504.

Richtmyer, R. D. and Morton, J. W., 1967: Difference Methods for Initial Value Problems, Interscience Publishers, 405 pp.

Walton, J. R., 1968: The validity of using smoothed topography for numerical weather prediction. M.S. Thesis, Univ. of Utah, Salt Lake City, Utah, 21 pp.

INITIAL DISTRIBUTION LIST

		No. Copies
1.	Defense Documentation Center Cameron Station Alexandria, Virginia 22314	2
2.	Library, Code 0212 Naval Postgraduate School Monterey, California 93940	2
3.	Naval Weather Service Command Washington Navy Yard Washington, D. C. 20390	1
4.	Professor G. J. Haltiner Department of Meteorology Naval Postgraduate School Monterey, California 93940	1
5.	Professor Roger T. Williams Department of Meteorology Naval Postgraduate School Monterey, California 93940	10
6.	Lieutenant James K. DeBoer, USN FWC/JTWC, Box 12 COMNAVMARIANAS Fleet Post Office San Francisco, California 96630	2
7.	Officer in Charge Navy Weather Research Facility Naval Air Station, Building R-48 Norfolk, Virginia 23511	1
8.	Commanding Officer Fleet Numerical Weather Central Naval Postgraduate School Monterey, California 93940	1
9.	Director, Naval Research Laboratory Attn: Tech. Services Info. Officer Washington, D. C. 20390	1
10.	Department of Meteorology Code 51 Naval Postgraduate School Monterey, California 93940	1

11. American Meteorological Society — 1
45 Beacon Street
Boston, Massachusetts 02128

12. Office of Naval Research — 1
Department of the Navy
Washington, D. C. 20360

13. Commander, Air Weather Service — 1
Military Airlift Command
Scott Air Force Base, Illinois 62226

14. Professor Victor Starr — 1
Department of Meteorology
M.I.T.
Cambridge, Massachusetts 03139

15. Dr. Joanne Simpson — 1
Experimental Meteorology Branch
Environmental Science Services Administration
Coral Gables, Florida 33124

16. National Center for Atmospheric Research — 1
Box 1470
Boulder, Colorado 80302

17. Dr. Fred Shuman — 1
Director, National Meteorological Center
Environmental Science Services Administration
Suitland, Maryland 20023

18. Dr. J. Smagorinsky — 1
Director, Geophysical Fluid Dynamics Laboratory
Princeton University
Princeton, New Jersey 08540

19. Professor N. A. Phillips — 1
54-1422
M.I.T.
Cambridge, Massachusetts 02139

20. Professor J. G. Charney — 1
54-1424
M.I.T.
Cambridge, Massachusetts 02139

21. Dr. M. G. Wurtele — 1
Department of Meteorology
U.C.L.A.
Los Angeles, California 90024

22. Dr. A. Arakawa — 1
Department of Meteorology
U.C.L.A.
Los Angeles, California 90024

23. Captain J. R. Walton, USAF — 1
USAF Environmental Technical Applications Center
Washington, D. C. 20330

24. Dr. J. W. Miles — 1
University of California
LaJolla, California 92037

25. Dr. J. D. Mahlman — 1
Geophysical Fluid Dynamics Laboratory
Princeton University
Princeton, New Jersey 08540

26. Dr. F. J. Winninghoff — 1
Department of Meteorology
Naval Postgraduate School
Monterey, California 93940

27. Dr. R. L. Elsberry — 1
Department of Meteorology
Naval Postgraduate School
Monterey, California 93940

28. Dr. R. L. Alberty — 1
Department of Meteorology
Naval Postgraduate School
Monterey, California 93940

29. Department of Meteorology — 1
University of Utah
Salt Lake City, Utah 84112

Security Classification

DOCUMENT CONTROL DATA - R & D

(Security classification of title, body of abstract and indexing annotation must be entered when the overall report is classified)

1. ORIGINATING ACTIVITY (Corporate author)	2a. REPORT SECURITY CLASSIFICATION
Naval Postgraduate School Monterey, California 93940	Unclassified
	2b. GROUP

3. REPORT TITLE

Numerical Simulation of Atmospheric Flow Over an Idealized Mountain

4. DESCRIPTIVE NOTES (Type of report and inclusive dates)

Master's Thesis; September 1970

5. AUTHOR(S) (First name, middle initial, last name)

James Keith DeBoer

6. REPORT DATE	7a. TOTAL NO. OF PAGES	7b. NO. OF REFS
September 1970	47	15

8a. CONTRACT OR GRANT NO.	9a. ORIGINATOR'S REPORT NUMBER(S)
b. PROJECT NO.	
c.	9b. OTHER REPORT NO(S) (Any other numbers that may be assigned this report)
d.	

10. DISTRIBUTION STATEMENT

This document has been approved for public release and sale; its distribution is unlimited.

11. SUPPLEMENTARY NOTES	12. SPONSORING MILITARY ACTIVITY
	Naval Postgraduate School Monterey, California 93940

13. ABSTRACT

The validity of linear smoothing of topography for numerical weather prediction and the variation of mountain drag with mountain height and static stability are examined in this study. In the model a constant geostrophic current is perpendicular to the mountain range and the height of the mountain is independent of y. The hydrostatic Boussinesq equations are used with motion bounded at the top by a rigid plane at z = D. A modified coordinate system similar to Phillips' sigma system was used. Solutions were obtained using a smoothed mountain profile. These solutions were compared with smoothed solutions obtained from the unsmoothed mountain. The comparison of these solutions shows that an error is introduced when non-linear terms become sufficiently large. Values of the mountain drag for differing values of mountain height at a given static stability and for differing values of static stability at a given mountain height were computed. Mountain drag was found to vary quadratically with mountain height and linearly with static stability.

DD FORM 1 NOV 68 1473 (PAGE 1)

S/N 0101-807-6811

Security Classification

A-31408

14 KEY WORDS	LINK A		LINK B		LINK C	
	ROLE	WT	ROLE	WT	ROLE	WT
Primitive equation model						
Mountain flow						
Mountain drag						